

Multi Degree of Freedom Hybrid FES and Robotic Control of the Upper Limb

Nathan Dunkelberger, *Member, IEEE*, Skye A. Carlson, Jeffrey Berning, Eric M. Schearer, and Marcia K. O’Malley, *Fellow, IEEE*

Abstract—Individuals who have suffered a spinal cord injury often require assistance to complete daily activities, and for individuals with tetraplegia, recovery of upper-limb function is among their top priorities. Hybrid functional electrical stimulation (FES) and exoskeleton systems have emerged as a potential solution to provide upper limb movement assistance. These systems leverage the user’s own muscles via FES and provide additional movement support via an assistive exoskeleton. To date, these systems have focused on single joint movements, limiting their utility for the complex movements necessary for independence. In this paper, we extend our prior work on model predictive control (MPC) of hybrid FES-exo systems and present a multi degree of freedom (DOF) hybrid controller that uses the controller’s cost function to achieve desired behavior. In studies with neurologically intact individuals, the hybrid controller is compared to an exoskeleton acting alone for movement assistance scenarios incorporating multiple degrees-of-freedom of the limb to explore the potential for exoskeleton power consumption reduction and impacts on tracking accuracy. Additionally, each scenario is explored in simulation using the models required to generate the MPC formulation. The two DOF hybrid controller implementation saw reductions in power consumption and satisfactory trajectory tracking in both the physical and simulated systems. In the four DOF implementation, the experimental results showed minor improvements for some joints of the upper limb. In simulation, we observed comparable performance as in the two DOF implementation.

Index Terms—functional electrical stimulation, upper limb, robotic exoskeleton, model predictive control, hybrid control, movement assistance

I. INTRODUCTION

SPINAL cord injury (SCI) affects approximately 291,000 people in the United States, with a majority of these individuals suffering from tetraplegia [1]. For this population,

This material is based upon work supported by the National Science Foundation under Grants NSF CBET 2025130 and 2025142. Any opinions, findings, and conclusions or recommendations expressed in this material are those of the authors and do not necessarily reflect the views of the National Science Foundation.

M. K. O’Malley, corresponding author, is with Rice University, Houston, TX 77005 USA (e-mail: omalleym@rice.edu).

N. Dunkelberger was with Rice University, Houston, TX 77005 USA. He is now with CACI International, Houston, TX 77058 USA, (e-mail: nathan.b.dunkelberger@nasa.gov).

J. Berning was with Rice University, Houston, TX 77005 USA. He is now with Burns & McDonnell, Kansas City, MO, 64114 USA, (e-mail: jberning@burnsmcd.com).

S. A. Carlson and E. M. Schearer are with Cleveland State University, Cleveland OH 44115 USA (e-mails: s.a.carlson@vikes.csuohio.edu and e.schearer@csuohio.edu).

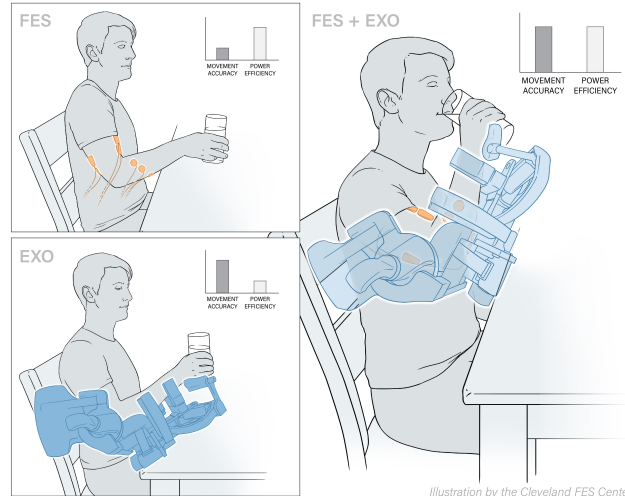


Illustration by the Cleveland FES Center

Fig. 1. An example application of hybrid FES and Exoskeleton systems. With FES alone, a user might have poor movement accuracy, and would therefore have difficulty completing tasks that require highly coordinated movements. With an exoskeleton alone, a user would be able to complete tasks with high accuracy, but the device would require significant power to move the entire upper limb, limiting the amount of time a portable system could be used before recharging. With a hybrid system, highly dexterous movements could be performed with high accuracy, with relatively low power consumption.

restoration of upper-limb function is one of the top priorities in regaining independence [2]. While some individuals with SCI may regain some amount of upper limb function from intensive rehabilitation, many individuals cannot regain function, and are therefore reliant on caregivers to help them perform activities of daily living (ADLs) [3].

Upper extremity exoskeletons and functional electrical stimulation (FES) are two technologies that aim to provide functional assistance for individuals with paralysis resulting from SCI, but neither of these technologies is able to meaningfully provide this assistance alone. Exoskeletons have inherently high power requirements and are bulky [4]–[7], which often limits their use to clinical settings. FES systems are well-suited to supporting gross movements such as grasping that do not require precision, and the inherent time delays that exist when electrically stimulating muscles to generate limb movements makes stable feedback control challenging [8], [9]. Hybrid control approaches that combine these two technologies are gaining traction because of their complementary strengths. In hybrid systems, illustrated in Fig. 1, FES can be used

for gross limb movements, while lightweight exoskeletons with embedded sensors can be used to assist with fine-tuned movements [10]–[14].

While this combination is promising, the hybrid implementation of FES and robotic exoskeletons introduces new challenges. For example, when combining two systems with differing dynamic characteristics, it is important to achieve a distribution of control effort that works to each of their strengths. Additionally, the reduction in power requirements cannot come at a cost of movement accuracy, because the upper-limbs require fine and coordinated movements to complete daily tasks. We have previously demonstrated the reduction of power consumption without significant loss in accuracy for a hybrid FES and exoskeleton system for the upper limb when completing single-DOF movements [15]. For practical applicability, it is important to extend this approach to multi-DOF movements necessary for functional assistance.

Multi-DOF implementation of hybrid FES and exoskeleton systems is challenging due to the complexities that arise when combining two already dynamically complex systems. Early attempts at using hybrid systems on the upper-limb for multi-DOF movements avoided these complexities by using each of the components independently. For example, some approaches use electromechanical actuation on some joints and FES on others [13], [16], [17]. Others use exoskeletons to restrict motion on some joints, allowing FES to act on one joint at a time [18], [19]; however, this simple combination does not achieve the proposed benefits of combining the two systems *on the same joints*. More recently, work has focused on achieving the benefits of combining FES and exoskeleton actuation on the same joint at the same time, with both experimental [5], [14], [20] and simulated [12] demonstrations. Each of these implementations only study the effect on a single-DOF at a time, and many of the algorithms presented in these studies do not readily translate to multi-DOF movements that are necessary for activities of daily living. Therefore, there is a need for hybrid control algorithms that have the ability to assist motion on several DOFs at the same time, and still provide the same benefits that have been observed in single-DOF implementations.

In this paper, we present the adaptation of a single-DOF hybrid FES and exoskeleton model predictive control (MPC) based controller, detailed in [15], to a multi-DOF implementation. We then evaluate this multi-DOF hybrid controller in both two-DOF and four-DOF implementations, and evaluate controller performance in a trajectory following task with neurologically intact participants. First, we test the hybrid controller without torque limits on the exoskeleton to understand the power consumption of the hybrid controller compared to an exoskeleton acting alone, without FES. Second, we evaluate the trajectory tracking performance of the hybrid controller with artificial torque limits imposed on the exoskeleton, emulating the performance capabilities of a less capable exoskeleton with components that mimic those more suited to wearable exosuits [21]–[23]. The dynamic models of the hybrid FES-exo system are also implemented in simulation to provide further insights on the differences between the hybrid controller behavior in an idealized simulation versus

that observed experimentally with able-bodied participants.

II. METHODS

A. Approach

The objective of this study is to demonstrate the performance of an MPC-based hybrid controller with the goal of effectively distributing actuation between FES and exoskeleton subsystems, while accurately tracking a multi-DOF trajectory. To develop the model for the MPC controller, we first generate a model of the torque output of the FES subsystem for a participant using recruitment curves to model the relationship between commanded pulse-width and muscle activation, and Gaussian process regression (GPR) models to predict the maximum output torque for each electrode given the joint configuration. This is used together with an identified dynamic model of the combined exoskeleton and arm to generate a full hybrid dynamic model which is used in the hybrid MPC scheme that uses a cost function to achieve the controller objectives. The developed hybrid controller is tasked to follow a multi-DOF trajectory and is compared to a controller that only uses an exoskeleton to complete movements using different combinations of DOFs. These controllers are tested in different scenarios that are designed to illustrate how the power consumption and tracking accuracy vary in different hybrid system configurations. Lastly, these scenarios are also explored in a simulation model to understand how an optimal system behaves, and learn where differences may exist between the model and the physical system.

B. Participants

Six neurologically intact participants (2 female, average age of 23.8, age range from 20 to 27) took part in this study. All participants had completed previous experiments with hybrid FES and exoskeleton systems, and provided informed consent for this study. The study protocols were approved by institutional review boards at Rice University (IRB #FY2017-461) and Cleveland State University (IRB #30213-SCH-HS).

C. Materials

The robotic device used for this study is the MAHI Open Exoskeleton [5]. The exoskeleton, pictured in Fig. 2A, has four degrees of freedom (DOF), namely elbow flexion/extension (EFE), forearm pronation/supination (FPS), wrist flexion/extension (WFE), and wrist radial/ulnar deviation (WRU). When these joints are referred to numerically in equations, the numbers correspond to the order they are listed, which is also the order from the most proximal to the most distal DOF. Each of the axes of the exoskeleton joints is aligned with the equivalent joint of the upper limb when fitted properly in the exoskeleton. With this in mind, in the generic dynamic equations, $\tau_{exo} \in \mathbb{R}^{4 \times 1}$ is the torque from the exoskeleton, and it is defined as the four torque inputs by motors acting on each of the joints.

The exoskeleton has several adjustable parameters that are set for each participant at the beginning of the study to ensure that their joints are aligned with the DOFs of the exoskeleton

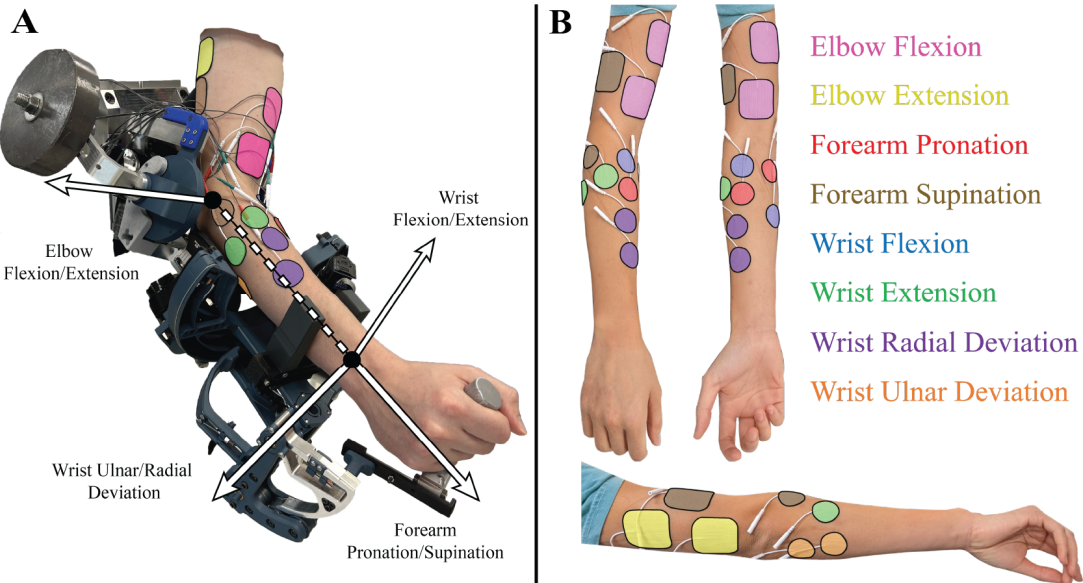


Fig. 2. Panel A: MAHI Open-Exo with participant. Panel B: Electrode placements on the upper limb of a participant, with each pair of electrodes corresponding to a single channel.

[5]. Additionally, the counterweight on the exoskeleton is adjusted such that EFE had a neutral position approximately -30° from horizontal when the arm is in the exoskeleton to require roughly even amounts of flexion and extension throughout the trajectory (see Fig. 2A).

FES is provided by a transdermic electrical stimulation system [24]. This system has eight bipolar output channels, each used to target either the positive or the negative direction of the four DOFs provided by the exoskeleton. The torques generated by the FES system on each of the four DOFs are referred to in a similar way as the exoskeleton torques, where $\tau_{fes} \in \mathbb{R}^{4 \times 1}$ refers to the torque provided on each of the joints due to the contributions of all FES channels. To provide variation in muscle response according to stimulation parameters, the amplitude and frequency of each stimulation channel are kept constant while the pulse-width is varied.

D. Model Characterization

Model characterization comprises several steps, including FES placement and threshold identification, recruitment curve characterization, Gaussian process regression model creation, and characterizing the dynamic model of the user's arm. We follow many of the same steps of that were detailed in our prior work for single DOF implementation of hybrid FES-Exo control [15]. For clarity, we detail here only those aspects of characterization that are significantly different when compared to our previous implementation. Additional details are included as Supplementary Materials.

1) FES Placement and Threshold Identification: Surface electrodes are placed on the participant's upper limb to deliver muscle stimulation patterns that generate desired movements. The specific placement of each electrode channel is based on pilot testing, and an example of electrode placement is shown in Fig. 2B. Electrode channels were placed four at a time with the arm outside of the robot, meaning that all

electrode channels for targeting EFE and FPS movement were placed first, followed by all electrode channels targeting WFE and WRU movement (see Supplementary Materials). After all electrodes were placed, the minimum and maximum pulse-width thresholds were found as presented in [15].

2) Recruitment Curve Characterization: A recruitment curve was generated for each electrode channel to determine the required stimulation pulse-width necessary to achieve a desired level of muscle activation, α . The process to generate a recruitment curve using the ramp deconvolution method [25] for an electrode is detailed in [15], and remained the same in this study. For details, see Supplementary Materials.

3) Gaussian Process Regression Model Creation: Gaussian Process Regression (GPR) models are used to estimate the torque output for each electrode along each of the four DOFs at maximum activation ($\alpha = 1$) for a given configuration, q [26]. GPR models are trained with inputs of 27 unique configurations, which are combinations of EFE, FPS, and WFE positions, and outputs of torque values along each of the four DOFs collected at each of the input configurations. The WRU DOF was not used as an input, and therefore remained at a nominal position because pilot testing indicated that WRU position had little effect on the GPR models, and eliminating this DOF from the process decreased the GPR model creation time which minimized the effects of fatigue on the muscles. For the three DOFs varied for training input data, each had three distinct positions, a minimum position, a maximum position, and a point halfway in between the minimum and maximum, with the 27 total points coming from the full factorial combination. The minimum and maximum positions chosen for each joint are the minimum and maximum values found in the trajectory that is used during the experiment, and spans a large portion of the comfortable range of motion.

The participant's arm was moved to each of the configurations in the exoskeleton, and when it arrived, the torque

along each DOF necessary to keep the system still without stimulation was recorded as $\tau_{passive} \in \mathbb{R}^{4 \times 1}$. At each position, each electrode channel was individually activated at maximum stimulation and the torque required to stay at that position once at steady state was recorded as $\tau_{hold} \in \mathbb{R}^{4 \times 1}$. The joint angles at each position and corresponding $\tau_{passive}$ and τ_{record} , defined in (1), were then used to fit the GPR models. The GPR models were then generated using Matlab's `fitrgp` with EFE, FPS, and WFE positions as input, and torque along a single DOF as the output.

$$\tau_{record} = \tau_{hold} - \tau_{passive} \quad (1)$$

The result of this fit is a matrix $P(q) \in \mathbb{R}^{4 \times 8}$ where entry (i, j) is a GPR model which takes inputs q and outputs the torque that electrode j will produce along DOF i if electrode j is commanded to an activation level of 1. Given this setup, the total torque applied by FES along the DOFs of the robot, given a vector of activation levels, α , can be described as

$$\tau_{fes} = P(q)\alpha. \quad (2)$$

4) Arm Model Characterization: To effectively use MPC, an accurate model of the dynamic system is required. The dynamics of the exoskeleton have been characterized in previous work [5], but the model did not include the mass properties of the arm, which are incorporated here. To characterize the mass properties of the arm, we assume that arm is composed of four joints that are rigidly attached to each of the joints on the exoskeleton. With this assumption, mass properties for each of the joints of the combined arm and exoskeleton system can be calculated by combining the already-characterized mass properties of the exoskeleton with newly characterized mass properties of the arm using the parallel axis theorem.

The process of identifying arm mass properties has been presented in previous work [15], but a slight modification is made to that protocol to identify arm mass properties in this study. In the previous study, while a single joint was tracking a chirp signal, the remainder of the joints remained in a locked position. In this study, each joint that is not commanded to track a chirp signal is commanded to follow sinusoidal profiles at various frequencies using independent PD controllers. This approach allows us to better generalize the mass properties across the full workspace, rather than over-fitting at the tested configurations. The mass properties of the combined arm and exoskeleton are used in the dynamic equations.

E. Hybrid Controller Design

We present the design of a hybrid FES and exoskeleton model predictive controller (MPC) that combines the efforts of FES and robot to act on four degrees-of-freedom of the upper limb. The design of the hybrid controller is similar to that presented in a previous study that examined the effects of single-DOF hybrid control [15]. For completeness, the controller design is presented here in its entirety.

To test the hybrid controller, three different versions of the controller are implemented and tested. These consist of 1) the EFE and FPS joints of the exoskeleton along with the four

TABLE I
HOLDING POSITION OF INACTIVE JOINTS THROUGHOUT TESTING.

Active Joints	q_{hold_1}	q_{hold_2}	q_{hold_3}	q_{hold_4}
EFE, FPS	N/A	N/A	0°	0°
WFE, WRU	-30°	-30°	N/A	N/A

electrode channels associated with those movements, 2) the WFE and WRU joints of the exoskeleton along with the four electrode channels associated with those movements, and 3) all four exoskeleton DOFs and all eight electrode channels. When a DOF combination does not use all DOFs, the inactive DOFs are held at q_{hold} values indicated in Table I using independent PD controllers on these exoskeleton joints.

The hybrid controller is presented in general terms for the 4-DOF use case with 4 exoskeleton DOFs active, and 8 electrode channels active. When the controller is implemented for the 2-DOF testing scenarios with 2 exoskeleton DOFs active and 4 electrode channels active, the same general formulations apply, but components of vectors or matrices related to the number of DOFs of movement will decrease from size 4 to size 2, and components related to the number of electrode channels active will decrease from size 8 to size 4.

In the four-DOF case, the dynamic equations appear as follows. Importantly, the dynamic equations use the lumped parameters for each of the degrees of freedom, as characterized in II-D.4. We define vectors of the exoskeleton positions, velocities, and accelerations as $q = [q_1, \dots, q_4]^T$, $\dot{q} = [\dot{q}_1, \dots, \dot{q}_4]^T$, and $\ddot{q} = [\ddot{q}_1, \dots, \ddot{q}_4]^T$ respectively.

$$\tau_{fes} + \tau_{exo} = M(q)\ddot{q} + V(q, \dot{q}) + G(q) + F_f(\dot{q}) \quad (3)$$

We previously characterized the FES torques given FES activations and joint configurations in Section II-D.3. Replacing τ_{fes} according to (2), we arrive at the following equation.

$$P(q)\alpha + \tau_{exo} = M(q)\ddot{q} + V(q, \dot{q}) + G(q) + F_f(\dot{q}) \quad (4)$$

The state, x , input, u and output, y of this hybrid system are described below, where C is a size 8 identity matrix and is the output matrix describing the variables we can observe.

$$x = [q^T, \dot{q}^T]^T \quad (5)$$

$$u_{exo} = [\tau_{exo_mpc_1}, \dots, \tau_{exo_mpc_4}]^T \quad (6)$$

$$u_{fes} = [\alpha_1, \dots, \alpha_8]^T \quad (7)$$

$$u = [u_{exo}^T, u_{fes}^T]^T \quad (8)$$

$$C = I_8 \quad (9)$$

$$y = Cx \quad (10)$$

We formulate our dynamics to use standard analyses:

$$\dot{x} = f(x, u) \quad (11)$$

To do this, we need an expression for \ddot{q} in terms of only x and u . We solve for \ddot{q} as follows.

$$\ddot{q} = M^{-1}(q)(P(q)\alpha + \tau_{exo} - V(q, \dot{q}) - G(q) - F_f(\dot{q})) \quad (12)$$

To reduce computational complexity, we utilize a linearized estimate of (11). This linearization about time k , is calculated as follows, where i is some time after k .

$$A_k = \frac{\partial f}{\partial x} \Big|_{x=x_k, u=u_k} \quad (13)$$

$$B_k = \frac{\partial f}{\partial u} \Big|_{x=x_k, u=u_k} \quad (14)$$

$$\dot{x}_i = A_k x_i + B_k u_i + \dot{x}|_{x=x_k, u=u_k} \quad (15)$$

This model of our dynamics is used in our MPC formulation. A cost function then needs to be defined that can choose control inputs based on the desired behavior for our hybrid system. We define the cost function evaluated at some time i given the estimate of system output, \bar{y}_i , system input, u_i , and desired state, r_i , as follows, where Δu_i is defined as $u_i - u_{i-1}$.

$$J_i = (r_i - \bar{y}_i)^T Q (r_i - \bar{y}_i) + \Delta u_i^T R \Delta u_i + u_i^T R_m u_i \quad (16)$$

In this cost function, $Q \in \mathbb{R}^{8 \times 8}$, $R \in \mathbb{R}^{12 \times 12}$, and $R_m \in \mathbb{R}^{12 \times 12}$ are all positive diagonal matrices. The specific components of the matrices are defined as follows.

$$Q = \text{diag}(Q_{q_1}, \dots, Q_{q_4}, Q_{\dot{q}_1}, \dots, Q_{\dot{q}_4}) \quad (17)$$

$$R = \text{diag}(R_{exo_1}, \dots, R_{exo_4},$$

$$R_{fes_1}, R_{fes_1}, \dots, R_{fes_4}, R_{fes_4}) \quad (18)$$

$$R_m = \text{diag}(R_{m_exo_1}, \dots, R_{m_exo_4},$$

$$R_{m_fes_1}, R_{m_fes_1}, \dots, R_{m_fes_4}, R_{m_fes_4}) \quad (19)$$

The entries of Q define the cost of trajectory tracking error, with higher values of Q_{q_i} and $Q_{\dot{q}_i}$ resulting in better tracking on joint i . Because the estimate \bar{y}_i is based on the model of the system, instability can arise in the presence of model error if the values of Q are set too high. The entries of R define the cost in the change in control input, which will result in smaller and smoother changes in input value u_i for higher values of the i th value on the diagonal of R . The entries of R_m define the cost in the magnitude of control input, which will result in lower magnitudes for input u_i for higher values of the i th value on the diagonal of R_m . As shown in (18) and (19), one gain is used for each exoskeleton torque input, and one gain is used for both of the activations for the electrodes that target the same DOF.

The desired behavior of the controller is for the FES to provide low frequency, high amplitude portions of the total torque, and for the exoskeleton to account for the high frequency, low amplitude portions of the total torque. This allows the exoskeleton torque to be reduced as much as possible, without causing unstable behavior due to the time delay in the FES actuation. To have the FES inputs provide lower frequency torque compared to the exoskeleton inputs, $R_{exo_i} \ll R_{fes_i}$, with each entry scaled for relative difference in expected torque magnitudes for DOF i . To achieve higher amplitude torques from the FES inputs compared to the exoskeleton inputs, $R_{m_fes_i} \ll R_{m_exo_i}$, again with each entry scaled for relative difference in torque magnitudes for DOF i .

The relative weighting between the different matrices also has a large affect on the behavior of the dynamic system. To ensure that trajectory tracking accuracy is not sacrificed to achieve the desired torque magnitude distributions, we keep $u_i^T R_m u_i \ll (r_i - \bar{y}_i)^T Q (r_i - \bar{y}_i)$.

The specific values for each of the gains in Q , R , and R_m were chosen based on pilot testing in simulation, then by fine tuning with participants on the physical system. The methodology in choosing these gains was to set Q and R to achieve stable behavior with RMS tracking error close to 1 degree on each DOF in simulation. Then, the R_m gains were chosen to achieve meaningful reduction in the exoskeleton torque, while maintaining tracking accuracy. As R_m gains were tuned, Q and R were further adjusted as necessary. Once gains were chosen, the controller was tested with participants in the experimental system, and gains were fine-tuned further.

The total cost function, J_{tot} is defined as the summation of the single point cost function over the prediction horizon, defined as N discretized points spaced T_s sections apart.

$$\underset{u(\cdot)}{\text{argmin}} J_{tot} = \sum_{i=1}^N J_{k+i} \quad (20)$$

subject to $\bar{y}_{i+1} = \bar{y}_i + T_s \dot{x}_i$,

$$0 \leq \alpha_e \leq 1, e = \{1, 2, \dots, 8\},$$

$$|\tau_{exo_mpc_m}| \leq \tau_{exo_max_m}, m = \{1, 2, 3, 4\}$$

This optimization is subject to the discretized integration of the estimate of the dynamics, the FES activation levels limited between 0 and 1, and the exoskeleton torques limited between $-\tau_{exo_max_m}$ and $\tau_{exo_max_m}$ for each τ_{exo_m} on DOF m .

The optimization problem described in (20) is created using the nonlinear optimization software CasADi [27] in C++. At runtime, the resulting dll file was then loaded and solved with the interior point optimizer, IPOPT [28].

Additional independent PID controllers were also used on each of the active joints with the goal of accounting for model error. The total exoskeleton torque provided to joint i , $\tau_{tot,i}$ is described as the summation of the MPC contribution of exoskeleton torque on joint i , $\tau_{exo_mpc,i}$, and the output of the PID controller on joint i , $\tau_{fb,i}$, but is still limited by the minimum and maximum values as described in (20). Because the feedback controller is intended to account for model error in the MPC formulation, the torques provided due to these feedback controllers were not provided to the MPC optimization. The overall control structure is shown in Fig. 3.

During data collection, the novel *hybrid controller* with shared actuation is compared against algorithms using the exoskeleton, which is called the *exoskeleton alone* controller. This control condition is implemented by simply changing the constraint on α in (20) to be $\alpha_e = 0$ where $e = \{1, 2, \dots, 8\}$. In this control condition, the R_{exo} control gains are chosen differently from the hybrid condition so that the tracking accuracy was similar in pilot testing.

F. Experimental Study Design

Once each of the model characterization steps were completed, the controller was compiled for each of the sets of

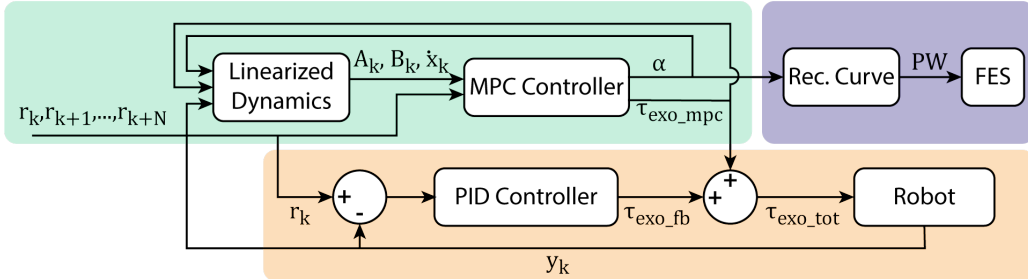


Fig. 3. The control diagram for the hybrid controller takes a reference trajectory, and provides desired exoskeleton torques and FES pulsewidths.

TABLE II
SUMMARY OF TEST CONDITIONS

Active DOFs	Unlimited Torque	Limited Torque
EFE, FPS	Hybrid	Hybrid
	Exo alone	Exo alone
WFE, WRU	Hybrid	Hybrid
	Exo alone	Exo alone
EFE, FPS, WFE, WRU	Hybrid	Hybrid
	Exo alone	Exo alone

active DOFs. The performance of the hybrid controller and exoskeleton alone controller were compared across a total of 36 trials performed with six neurologically intact individuals. In these trials, the first 18 were performed without any constraints on the exoskeleton joint torques, e.g. $\tau_{exo_max_m} = \infty$ in (20). This condition is intended to test power reduction potential if there are no limits on actuator capabilities. These first 18 trials were evenly split between the three different available DOF combinations with six trials for each. In each of these sets of six trials, three were run with the hybrid controller, and three were run with the exoskeleton alone controller.

After the first 18 trials were completed, the mean torque profiles for each joint in each of the DOF combinations for the exoskeleton alone controller were calculated. The maximum absolute value of torque used along each joint in each DOF combination was taken from these profiles and $\tau_{exo_max_m}$ for the remaining control conditions was set to half of the maximum value, allowing us to observe the difference in trajectory tracking capability between the hybrid controller and the exoskeleton alone controller in a scenario where torque is limited, as we might expect in future portable systems. The final 18 trials followed the same pattern as the first 18, now with torque constraints imposed. A summary of test conditions is presented in Table II.

Each trial followed the same artificially designed trajectory, which is composed of the addition of sinusoidal waves of various amplitudes and frequencies over a period of 42.4 seconds as in [15]. The trajectories can be seen in the figures representing the trajectory tracking accuracy results (Fig. 5). As each trial was performed, total robot torque commanded, position, and velocities of each DOF, as well as the commanded FES pulse-widths were recorded at a rate of 1 kHz using a Quanser Q8usb data acquisition device.

G. Simulation Study Design

In addition to the experiments with six neurologically intact participants, the models that were characterized for each participant were also tested in a simulation environment. This provides an opportunity to explore how the hybrid controller would operate in ideal conditions where the model used in the controller is exactly the same as the system being tested.

The exoskeleton simulation is the same as that presented in [5] but with the arm model parameters as presented in this study also incorporated into the dynamic model. To simulate the time delay characteristics of the FES system, the time delay between commanded stimulation and torque output due to FES is first estimated from the commanded impulses in the recruitment curve calibration for each electrode. When running the simulation, commanded activations are delayed by this amount before being provided as an input, and integrated into the dynamic equations as described in (4). To perform the data collection with the simulation, each of the control conditions in the unlimited torque case is tested a single time in the simulation environment. Only one repetition is used because additional repetitions would result in the same outcome in the idealized environment. For the trials with limited exoskeleton torque, the same procedure is used to calculate $\tau_{exo_max_m}$, but instead using the data collected in simulation.

H. Data Analysis

Each of the data analysis procedures was completed for the data collected from the experimental system and for the data collected from the simulation environment. The simulated systems only have one trial for each control condition, so averaging across trials was not necessary.

To understand how exoskeleton power consumption differs using the hybrid controller compared to using the exoskeleton alone controller, the data collected from the unlimited exoskeleton torque trials were analyzed. The joint-level sum of squared exoskeleton torques were first computed for each of the control conditions as described in [15], for each set of active joint combinations. This was calculated first at a participant level, where the sum of squared torques is calculated for each of the trials and then averaged for each condition to obtain a single value for each control condition per participant. Because the required torque profile to move through a trajectory will differ between participants due to different arm sizes and exoskeleton configurations, the data needs to be normalized to fairly compare between participants.

To do this, the percent improvement was calculated as in [15], where the percent improvement signifies a percentage reduction in power consumed on that specific joint. The individual participant data are represented in Fig. 4. A paired t-test was performed to understand whether there was a statistically significant difference in sum of squared torque between the exoskeleton alone and hybrid control conditions.

To evaluate trajectory tracking performance with the hybrid controller when the maximum allowed exoskeleton torque was decreased, the RMS tracking error was calculated in each control condition when the maximum allowable exoskeleton torque was artificially limited. RMS tracking error was calculated as in [15]. The tracking error averaged across participants for each controller and each condition is presented in Table III. A paired t-test was performed to determine whether there was a statistically significant difference in RMS tracking error between the exoskeleton alone and hybrid control conditions.

III. RESULTS

The reductions of the sum of squared torque from exoskeleton alone control to hybrid control are summarized in Fig. 4, with statistically significant results represented by purple stars. The results for the EFE/FPS DOF combination show that most of the benefit of the hybrid controller comes from the EFE joint, with a larger benefit shown in the simulated case. There were only slight changes from the exoskeleton-alone condition in the FPS joint when using the hybrid controller, and the magnitude of these results were lower than the standard error in both experimental and simulated systems. In the WFE/WRU combination, each DOF had a benefit in both the experimental and simulated system. In the experimental system, the hybrid controller showed more benefits in the WRU joint than the WFE joint, but also demonstrated a higher standard error, showing greater variability between participants. The simulated system showed larger benefits than the experimental system, with similar benefits on each of the DOFs and a larger standard error for the WRU joint.

When all 4 DOFs were active, the experimental and simulated systems showed different reductions in sum of squared torque. In this condition, the EFE joint had a reduction in sum of squared torques with the hybrid controller, with the simulation providing more than double the benefit compared to the experimental system. In the other joints, the hybrid controller used more power on average than the exoskeleton alone controller in the experimental system, while the hybrid controller used less power compared than the exoskeleton alone controller in the simulated system. Results for the WFE and WRU joints for the physical system have large standard errors, showing wide variability between participants.

The RMS tracking error was analyzed for the trials where maximum actuator torque was capped. Results are shown in Table III, with statistically significant results represented by stars in the Diff columns. Sample trajectories are presented in Fig. 5. In the EFE/FPS case, roughly a 50% improvement in RMS tracking error was achieved when using the hybrid controller in comparison to the exoskeleton alone controller in the EFE joint for both the experimental and simulated

cases. This brought the RMS error close to 2° in both the experimental and simulated systems. The FPS joint shows only a mild improvement, leaving the RMS error still at 12.1° in the experimental system, and 8.2° in the simulated system.

In the WFE/WRU case, the hybrid controller achieved a greater than 50% improvement in each of the joints in both the simulated and experimental systems, and the simulated systems showed higher percentages of improvement in each DOF. In the WFE/WRU case, the RMS errors were similar in the experimental and simulated systems for the WRU DOF, but the errors in the WFE simulated system were reduced from the experimental system in both controllers.

When all 4 DOFs were active, the RMS errors in the experimental and simulated systems were similar for the exoskeleton alone condition. In the simulated system, the hybrid controller was able to reduce the RMS error to below 2° for the EFE and WRU joints, and to below 4° for the WFE joint, while the FPS joint saw no change. In the experimental system, the hybrid controller did not produce as meaningful results. The EFE joint was reduced to 3° RMS error, but the RMS error in the remaining joints remained over 8° . The WRU joint had worse mean accuracy with the hybrid controller, unlike in simulation.

IV. DISCUSSION

Using hybrid FES and exoskeleton systems to provide upper limb movement assistance has been a topic of interest in recent years. To date, these studies have targeted moving a single DOF at a time, and many of the algorithms used do not translate to dynamically complex multi-DOF movements. In this paper, we have presented a multi-DOF, MPC-based, hybrid controller that distributes actuation between FES and an exoskeleton to assist users in completing upper limb movements. We tested the hybrid controller with six neurologically intact participants in a trajectory tracking task using different combinations of DOFs to evaluate how it performs in comparison to a controller that only uses the exoskeleton for movement assistance. These controllers were also tested in simulations employing the dynamic models used to generate the controllers. Data were analyzed to explore the controller's capabilities in reducing power consumption and improving tracking accuracy compared to an exoskeleton alone controller.

A. Power Reduction with Hybrid Control

Power consumption is crucial in determining the portability of potential assistive devices, because decreased power consumption can enable the use of smaller batteries, or can result in device operation over longer periods of time for the same battery size. To analyze power reduction, the reductions in sum of squared torque results are shown in Fig. 4. Reductions in power requirements for the hybrid controller were observed for three of the four DOFs of the exoskeleton for the two-DOF cases. The results for the experimental system demonstrate that the hybrid controller was able to achieve the desired behavior of reducing power consumption, indicating the potential of using more portable solutions to assist upper limb movements. Section IV-C specifically addresses the results for the FPS joint where reductions were not observed. These observed power

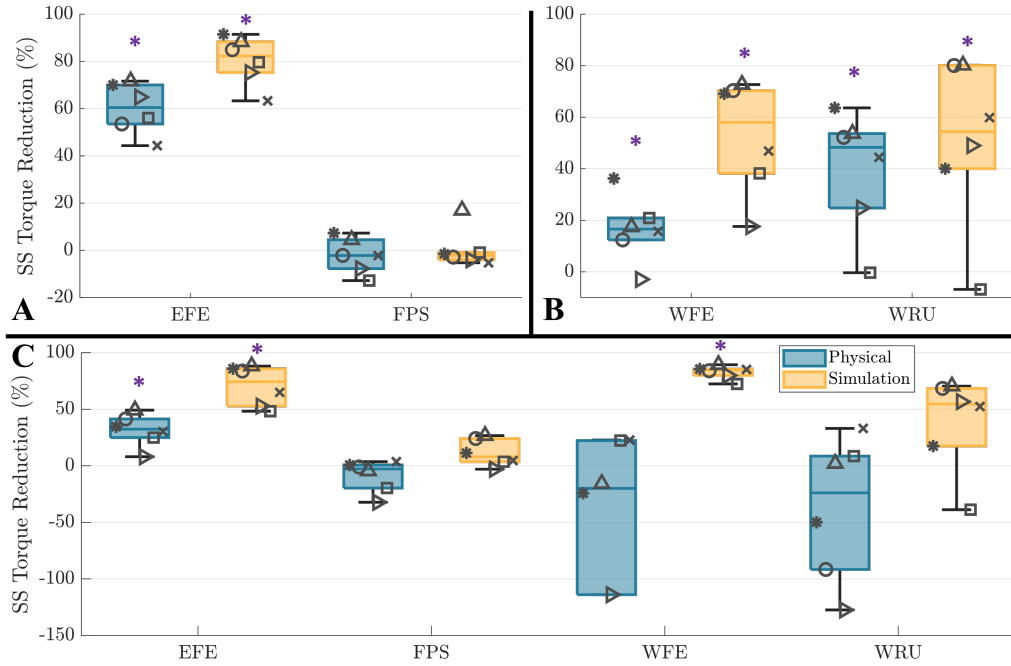


Fig. 4. Boxplots show the distribution of sum of squared torque reduction for each joint in the (A) EFE and FPS control case, (B) WFE and WRU control case, and (C) all four DOFs control case. Results with the physical experimental system are shown for data collected with unimpaired participants, and simulation results are shown for data collected using simulations of the models of subsystems. One outlier is not included in the graph to increase legibility, with the participant represented by the o symbol in the WFE physical case on plot (C) having a value of -373%. Plots with a purple * above them represent statistically significant results.

RMS TRACKING ERROR RESULTS FOR EACH CONTROL CONDITION, WITH STANDARD ERROR SHOWN IN PARENTHESIS, AND THE DIFFERENCE BETWEEN THE CONTROL CONDITIONS WITH PERCENT CHANGE IN PARENTHESIS, USING THE TRIALS WITH ARTIFICIALLY LIMITED TORQUE. RESULTS IN THE DIFF COLUMN WITH A * REPRESENT STATISTICALLY SIGNIFICANT RESULTS.

Active DOFs	Result DOF	Physical			Simulation		
		Exo Alone	Hybrid	Diff	Exo Alone	Hybrid	Diff
EFE/FPS	EFE	4.16° (0.42°)	2.08° (0.14°)	-2.08° (-49.9%)*	3.73° (0.15°)	1.70° (0.14°)	-2.03° (-54.4%)*
	FPS	13.07° (1.39°)	12.1° (1.54°)	-0.97° (-7.4%)	8.31° (0.36°)	8.17° (0.58°)	-0.14° (-1.7%)
WFE/WRU	WFE	10.07° (0.92°)	4.46° (0.69°)	-5.61° (-55.7%)*	4.07° (0.66°)	1.58° (0.62°)	-2.49° (-61.2%)*
	WRU	7.28° (0.57°)	3.28° (1.07°)	-4.00° (-55.0%)*	8.22° (0.81°)	2.34° (1.43°)	-5.88° (-71.6%)*
All DOF	EFE	4.42° (0.44°)	3.01° (0.48°)	-1.41° (-31.9%)*	4.00° (0.09°)	1.83° (0.29°)	-2.17° (-54.3%)*
	FPS	10.20° (0.86°)	9.73° (0.82°)	-0.48° (-4.7%)	7.33° (0.28°)	7.33° (0.48°)	-0.00° (-0.0%)
	WFE	9.45° (0.82°)	8.07° (2.29°)	-1.38° (-14.6%)	10.57° (1.39°)	1.46° (0.28°)	-9.11° (-86.2%)*
	WRU	7.71° (0.64°)	8.72° (1.64°)	+1.01° (+13.1%)	6.92° (0.76°)	3.82° (1.17°)	-3.11° (-44.9%)

reductions from the 2-DOF cases did not transfer well to the 4-DOF scenario, where there was a much greater variability in results; however, even though the average result showed that the hybrid controller increased power consumption, a reduction in power consumption was observed for some participants using the hybrid controller. In the two DOFs where the results were most variable (WFE and WRU), there seemed to be a trend across participants where some consistently demonstrated reductions in power while others did not. This might indicate that there are some participants who are better suited to a hybrid approach to movement assistance than others, which should be explored in greater detail in the future.

In each of the combinations of DOFs, the simulation results showed better power reduction performance compared to the experimental system, and the power consumption reduction was observed in both 2-DOF and 4-DOF cases. In these

idealized conditions, the hybrid controller is able to achieve the desired outcome, which shows promise if we can more accurately model the human-robot dynamic system. Section IV-D presents further analysis of the comparisons between simulation and experimental results. For additional analysis of the resulting torque profiles, see the Supplementary Materials.

B. Trajectory Tracking Accuracy

Trajectory tracking accuracy is important for realizing co-ordinated assistive movements of the upper limb. In a future where portable exoskeletons may not have the same maximum torque output as our grounded, rigid exoskeleton, we still aim to achieve accurate tracking. Analyzing the RMS error for the artificially torque-limited 2-DOF cases, satisfactory tracking performance is observed on each DOF except for FPS. As seen in the plots for WFE and WRU trajectory tracking shown in

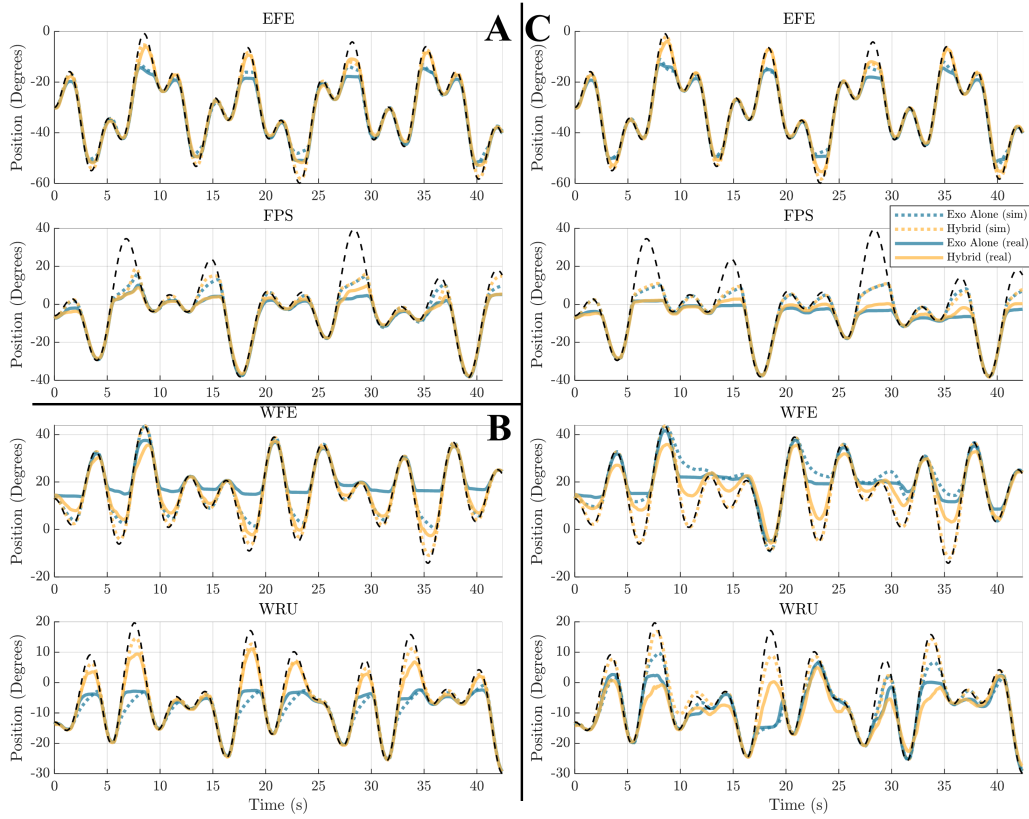


Fig. 5. Trajectories for the EFE and FPS (A), and WFE and WRU trajectories (B) in the two-DOF implementations, and for all DOFs in the four-DOF implementation (C) are shown, for both the hybrid controller and exoskeleton alone controller in cases where torque is artificially limited. The reference trajectory is shown by the black dashed line. In the two-DOF cases, the hybrid controller is able to better follow the trajectory in each of the DOFs, except for FPS while in the four-DOF case, the hybrid controller benefit is not as clear.

Fig. 5B, the exoskeleton is limited when it cannot overcome gravity, while the hybrid controller is able to expand the available workspace when trying to follow a complex trajectory. This shows promise that in the future, lightweight systems with limited torque can achieve more accurate trajectory following and reach more of a usable workspace in a hybrid system compared to using an exoskeleton alone. This finding did not hold for the 4-DOF case. We see in Fig. 5C that for some portions of trajectories, the hybrid controller is able to effectively expand the range of motion towards the extremes, but at some points, the hybrid controller achieves a smaller range of motion compared to the exoskeleton alone. In the current controller design and implementation, as more DOFs are incorporated, the controller cannot reliably provide the additional tracking accuracy that is desired. In contrast, the simulated results show similarly good benefits in the 4-DOF case compared to the 2-DOF case, meaning that in an idealized scenario with a perfect model of the system, the controller behavior is able to effectively follow these trajectories when the exoskeleton cannot do it by itself.

C. Non-ideal Performance in Pronation-Supination

There was consistently a lack of any benefit provided to the FPS joint using the hybrid controller. This is largely due to the fact that the torques generated along the FPS DOF by the electrodes were much smaller compared to the rest of the

DOFs. Due to the way the cost function is created, if the tracking accuracy or exoskeleton torque on other joints would have to be sacrificed to achieve better results for FPS, the algorithm would prefer to see no result on that joint. While this appears to be hurting the results in this study, this is actually a benefit of having the torques on all relevant DOFs represented in the GPR calibration, so that the full effect of commanded FES activations can be taken into account. In this experiment, the cost function weighting parameters were chosen to be scaled according to typical torque outputs on each joint, but the hybrid controller has the flexibility to modify weighting parameters if a specific task requires increased or decreased FES assistance for a specific DOF. The insight from this could additionally aid the design of future hybrid systems. For example, because the available FES torque production from the FPS joint is generally quite low, wearable system designers can provide greater torque capabilities for that DOF so that FES does not have to make up as much of the work.

D. Experimental and Simulation Mismatch

The results in the simulated and experimental systems differ, especially in the 4-DOF case. Two independently developed models are used to create the full dynamic model (FES and arm with exoskeleton) and model inaccuracies likely contribute to the overall mismatch in results. To analyze the accuracy of the dynamic model for the arm and exoskeleton

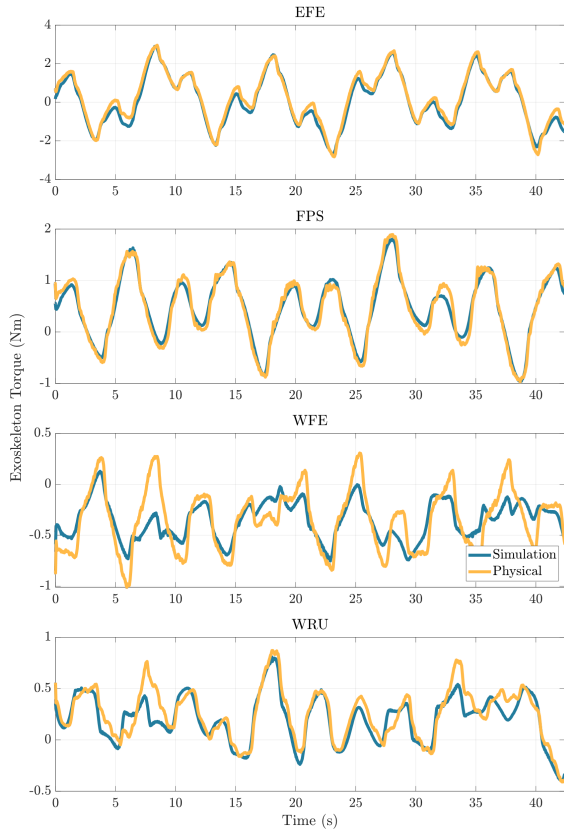


Fig. 6. The exoskeleton torque required to move in the 4-DOF case in the exoskeleton alone control condition is averaged across all participants for the simulated system (blue) and the experimental physical system (yellow), for each of the DOFs. These two profiles match well, showing the accuracy of the generated dynamic model.

subsystems, we compare the exoskeleton joint-level torques required to move the arm and exoskeleton through the trajectory for the experimental and simulated systems. Because the simulated system is based on the characterized dynamic model of the arm and exoskeleton, the torque profiles should be the same to provide the same movement, and differences in required torque profiles can be attributed to model error of the arm and exoskeleton dynamic characterization.

This is seen in Fig. 6, where the torque profiles are averaged across all participants. These results show general agreement in shape and magnitude across all four torque profiles, although the WFE profile has greater differences compared to the other DOFs, especially at the extremities of the trajectory. The relative agreement between these two results indicate that differences between the experimental and simulation results are not largely attributable to error in the dynamic model of the robot and arm, although the modeling of the WFE joint could be contributing to some of the discrepancies in that joint.

We cannot directly measure the torque output of the FES subsystem alone throughout the motion. Considering the system dynamics (Equation (3)), each of the terms except for τ_{fes} are accounted for in Fig. 6. It is likely that an inaccurate model of FES torque results in poorer performance of the controller in the more complex 4-DOF scenarios.

There are several potential sources of error that should be explored in future work. One of the primary assumptions of

the FES model is that the electrodes can be characterized as activating one muscle at a time, and that the individual characterizations can be summed to arrive at the total response. This assumption may hold relatively well for single DOF movements (as in [15]) and for 2-DOF movements because there are not as many electrodes activated at the same time. For the complex 4-DOF movements where more electrodes are active at a time, the stimulation from electrodes can radiate out and impact multiple muscles. This could be compounded by the fact that recruitment curves are nonlinear. Further assumptions are made in the GPR models, where we only characterized the torque production at 27 discrete locations in the workspace, and only used 3 of the 4 available positions to inform the model. Additionally, only the position values are used, but according to the Hill-type muscle model, velocities would also likely contribute to the muscle activation dynamics [29]. If more training points could be incorporated or if velocity of joints could be integrated into the training data without causing fatigue due to long characterization times, the FES model would also likely increase in accuracy. These insights show the need for better characterization of FES models, specifically in cases where many electrodes are active.

V. CONCLUSION

In this paper, we presented the implementation of a model-based hybrid controller for multi-DOF coordinated movements of the upper limb in neurologically intact participants. We tested the hybrid controller for trajectories that used combinations of two and four DOFs of the exoskeleton, and examined performance experimentally, as well as in simulation. The controller was tested without limits on exoskeleton torque to understand power reduction compared to an exoskeleton alone control implementation. We also tested the controller with imposed limits on exoskeleton torque to understand how performance might be impacted for a case that is representative of future portable hybrid devices that may have limited power. In the cases with two joints active, the hybrid controller was able to improve the target metrics on every joint except for FPS in the experimental system. Similar results were seen in the simulated system, but with greater benefits in all cases. In the cases with all four joints active, only the EFE joint saw improvements in the main objectives when using the hybrid controller, while controller performance on the remainder of the joints resulted in varying levels of improvement, and in some cases the performance decreased. In the simulated case, improvement was seen across all joints for both control conditions, except for the FPS joint, which showed no change. The improvements seen in the two-DOF cases in both simulation and the experimental system show how this hybrid controller can be beneficial compared to an exoskeleton alone for movement assistance, if the complexity of the trajectories remains limited. The simulated results in the four DOF case show that the controller has the desired behavior when the dynamic model used in the controller is accurate, but further improvements are needed to achieve these results in experimental hybrid control scenarios.

REFERENCES

- [1] NSCISC, "Spinal cord injury facts and figures at a glance," National Spinal Cord Injury Statistical Center, 2019.
- [2] K. D. Anderson, "Targeting recovery: Priorities of the spinal cord-injured population," *Journal of Neurotrauma*, vol. 21, no. 10, pp. 1371–1383, 2004.
- [3] J. L. Collinger, M. L. Boninger, T. M. Bruns, K. Curley, E. Wang, and D. J. Weber, "Functional priorities, assistive technology, and brain-computer interfaces after spinal cord injury," *Journal of Rehabilitation Research and Development*, vol. 50, no. 2, pp. 145–160, 2013.
- [4] R. Gopura, D. Bandara, K. Kiguchi, and G. K. Mann, "Developments in hardware systems of active upper-limb exoskeleton robots: A review," *Robotics and Autonomous Systems*, vol. 75, pp. 203–220, 2016.
- [5] N. Dunkelberger, J. Berning, K. J. Dix, S. A. Ramirez, and M. K. O'Malley, "Design, characterization, and dynamic simulation of the mahi open exoskeleton upper limb robot," *IEEE/ASME Transactions on Mechatronics*, vol. 27, no. 4, pp. 1829–1836, 2022.
- [6] B. Kim and A. D. Deshpande, "An upper-body rehabilitation exoskeleton harmony with an anatomical shoulder mechanism: Design, modeling, control, and performance evaluation," *The International Journal of Robotics Research*, vol. 36, no. 4, pp. 414–435, 2017.
- [7] Hocoma, "ArmeoPower," hrefhttps://www.hocoma.com/us/solutions/armeo-power/, accessed: 11/27/2017.
- [8] C. L. Lynch and M. R. Popovic, "Functional electrical stimulation," *IEEE Control Systems Magazine*, vol. 28, no. 2, pp. 40–50, Apr 2008.
- [9] C. S. Bickel, C. M. Gregory, and J. C. Dean, "Motor unit recruitment during neuromuscular electrical stimulation: a critical appraisal," *European journal of applied physiology*, vol. 111, no. 10, p. 2399, 2011.
- [10] N. Dunkelberger, E. M. Schearer, and M. K. O'Malley, "A review of methods for achieving upper limb movement following spinal cord injury through hybrid muscle stimulation and robotic assistance," *Experimental Neurology*, vol. 328, p. 113274, 2020.
- [11] N. Dunkelberger, S. A. Carlson, J. Berning, K. C. Stovicek, E. M. Schearer, and M. K. O'Malley, "Shared control of elbow movements with functional electrical stimulation and exoskeleton assistance," in *2022 International Conference on Rehabilitation Robotics (ICORR)*, 2022, pp. 1–6.
- [12] E. Bardi, S. Dalla Gasperina, A. Pedrocchi, and E. Ambrosini, "Adaptive cooperative control for hybrid fes-robotic upper limb devices: a simulation study," in *2021 43rd Annual International Conference of the IEEE Engineering in Medicine and Biology Society (EMBC)*, 2021, pp. 6398–6401.
- [13] A. B. Ajiboye, F. R. Willett, D. R. Young, W. D. Memberg, B. A. Murphy, J. P. Miller, B. L. Walter, J. A. Sweet, H. A. Hoyen, M. W. Keith *et al.*, "Restoration of reaching and grasping movements through brain-controlled muscle stimulation in a person with tetraplegia: a proof-of-concept demonstration," *The Lancet*, vol. 389, no. 10081, pp. 1821–1830, 2017.
- [14] D. Burchielli, N. Lotti, F. Missiroli, C. Bokranz, A. Pedrocchi, E. Ambrosini, and L. Masia, "Adaptive hybrid fes-force controller for arm exosuit," in *2022 International Conference on Rehabilitation Robotics (ICORR)*, 2022, pp. 1–6.
- [15] N. Dunkelberger, J. Berning, E. M. Schearer, and M. K. O'Malley, "Hybrid fes-exoskeleton control: Using mpc to distribute actuation for elbow and wrist movements," *Frontiers in Neurorobotics*, vol. 17, p. 1127783, 2023.
- [16] S. Schulz, S. B. W. R. C. Pyatiuk, and M. Reischl, "The hybrid fluidic driven upper limb orthosis - orthojacket," *Proceedings of the 2011 MyoElectric Controls/Powered Prosthetics Symposium Fredericton*, 08 2011.
- [17] R. Varoto, E. S. Barbarini, and A. Cliquet, "A hybrid system for upper limb movement restoration in quadriplegics," *Artificial Organs*, vol. 32, no. 9, pp. 725–729, 2008.
- [18] E. Ambrosini, S. Ferrante, J. Zajc, M. Bulgheroni, W. Baccinelli, E. D'Amico, T. Schauer, C. Wiesener, M. Russold, M. Gfoehler, M. Puchinger, M. Weber, S. Becker, K. Krakow, M. Rossini, D. Prosperi, G. Gasperini, F. Molteni, G. Ferrigno, and A. Pedrocchi, "The combined action of a passive exoskeleton and an EMG-controlled neuroprosthesis for upper limb stroke rehabilitation: First results of the RETRAINER project," *IEEE International Conference on Rehabilitation Robotics*, pp. 56–61, 2017.
- [19] C. Klauer, T. Schauer, W. Reichenfelser, J. Karner, S. Zwicker, M. Gandomi, E. Ambrosini, S. Ferrante, M. Hack, A. Jedlitschka, A. Duschau-Wicke, M. Gföhler, and A. Pedrocchi, "Feedback control of arm movements using neuro-muscular electrical stimulation (nmes) combined with a lockable, passive exoskeleton for gravity compensation," *Frontiers in Neuroscience*, vol. 8, no. 262, pp. 1–16, 2014.
- [20] D. Wolf, N. Dunkelberger, C. G. McDonald, K. Rudy, C. Beck, M. K. O'Malley, and E. Schearer, "Combining functional electrical stimulation and a powered exoskeleton to control elbow flexion," in *2017 International Symposium on Wearable Robotics and Rehabilitation (WeRob)*, Nov 2017, pp. 1–2.
- [21] Z. Kadivar, C. E. Beck, R. N. Rovekamp, M. K. O'Malley, and C. A. Joyce, "On the efficacy of isolating shoulder and elbow movements with a soft, portable, and wearable robotic device," in *Wearable Robotics: Challenges and Trends*. Springer, 2017, pp. 89–93.
- [22] Z. Kadivar, C. E. Beck, R. N. Rovekamp, and M. K. O'Malley, "Single limb cable driven wearable robotic device for upper extremity movement support after traumatic brain injury," *Journal of Rehabilitation and Assistive Technologies Engineering*, vol. 8, p. 20556683211002448, 2021.
- [23] F. Missiroli, N. Lotti, E. Tricomi, C. Bokranz, R. Alicea, M. Xiloyannis, J. Krzywinski, S. Crea, N. Vitiello, and L. Masia, "Rigid, soft, passive, and active: A hybrid occupational exoskeleton for bimanual multijoint assistance," *IEEE Robotics and Automation Letters*, vol. 7, no. 2, pp. 2557–2564, 2022.
- [24] S. C. Trier, J. R. Buckett, A. Campean, M. E. Miller, F. W. Montague, T. L. Vrabec, J. A. Weisgarber, and C. F. Center, "A modular external control unit for functional electrical stimulation," in *Proceedings of the 6th Annual Conference of the International Functional Electrical Stimulation Society*, vol. 2001, 2001, pp. 16–20.
- [25] W. Durfee and K. MacLean, "Methods for estimating isometric recruitment curves of electrically stimulated muscle," *IEEE Transactions on Biomedical Engineering*, vol. 36, no. 7, pp. 654–667, 1989.
- [26] E. M. Schearer, Y. Liao, E. J. Perreault, M. C. Tresch, W. D. Memberg, R. F. Kirsch, and K. M. Lynch, "Semiparametric identification of human arm dynamics for flexible control of a functional electrical stimulation neuroprosthesis," *IEEE Transactions on Neural Systems and Rehabilitation Engineering*, vol. 24, no. 12, pp. 1405–1415, 2016.
- [27] J. A. E. Andersson, J. Gillis, G. Horn, J. B. Rawlings, and M. Diehl, "CasADI – A software framework for nonlinear optimization and optimal control," *Mathematical Programming Computation*, vol. 11, no. 1, pp. 1–36, 2019.
- [28] A. Wächter and L. T. Biegler, "On the implementation of an interior-point filter line-search algorithm for large-scale nonlinear programming," *Mathematical Programming*, vol. 106, no. 1, pp. 25–57, Mar 2006.
- [29] A. van den Bogert, K. Gerritsen, and G. Cole, "Human muscle modelling from a user's perspective," *Journal of Electromyography and Kinesiology*, vol. 8, no. 2, pp. 119–124, 1998. [Online]. Available: <https://www.sciencedirect.com/science/article/pii/S105064119700028X>